CRYSTALLIZATION KINETICS OF Al_2O_3-CaO-SiO_2 BASED OXIDE INCLUSIONS

P. Rocabois, J. N. Pontoire, J. Lehmann, H. Gaye,
IRSID, BP 30320, Maizières-les-Metz, F-57283, France

Abstract

The crystallization kinetics of various oxides melts based in the systems Al_2O_3-CaO-SiO_2-X (with X= MgO, Na_2O, CaF_2, TiO_2, ZrO_2) has been investigated and the Time-Temperature-Transformation curves have been drawn. The glass forming ability is characterized by temperature ranges of crystallization, incubation times or critical cooling rates. The main factors affecting the glass forming ability are the viscosity and the liquidus temperature of the melts. The effect of TiO_2 and ZrO_2 as nucleating agents was tested in a Al_2O_3-CaO-SiO_2-Na_2O-CaF_2 melts. The aim of this study is to better define the slag and flux compositions used for steelmaking and to better understand the rheology of the oxide inclusions in steel during hot rolling.

Introduction

Non metallic inclusions in solid steel may affect the physical and mechanical properties of the products and consequently their service properties. Obtaining clean steel is one of the goals of the steelmakers, however complete elimination of inclusions is not possible [1]. The harmfulness of these inclusions depends on their composition, size, position in the solidified steel, rheology during hot rolling and the final shape and application of the steel product itself[2,3]. Concerning long product, such as tire cord steel or valve spring steel, only endogenous inclusions that deform during hot rolling can be tolerated. Concerning flat products such as beverage can, mold flux droplets trapped during continuous casting and further deformed during the rolling steps may cause surface defects which appear during stamping. These two examples show that, depending on the steelgrade and the final service properties, different rheologies of oxide inclusions are harmful.

The rheology of inclusions largely depends on their crystallization state: amount, morphology and nature of the crystals. Some oxide mixtures can form metastable supercooled liquids down to 600-900°C. However, these metastable liquids, that form a glassy phase at lower temperatures, remain susceptible of crystallizing during heat treatment before hot rolling. It thus appears necessary to better understand the kinetics of crystallization of various oxide melts encountered in steels and to determine which compositions are the least harmful with respect to the thermal history, the shaping and the field of application of the product.

In this paper, we present our experimental technique and discuss the crystallization mechanisms of various oxide melts as deduced from our results.

Experimental

The crystallization of inclusions may be studied on the industrial product or using synthetic inclusions of the same composition. The interest of the laboratory study of synthetic inclusions is:

- a known and controlled initial composition;
- a large volume making it possible to show the homogeneous or heterogeneous nucleation phenomena, including for a low nucleation rate;
- the growth of crystals unlimited by the volume;
- the greater possibilities for characterization (SEM/EDS, X-ray diffraction, optic microscope, image analysis).

The technique consists in preparing glassy homogeneous mixtures, placing them in welded steel crucibles, then making heat treatments, followed by quenching. The results are given in the form of a TTT curve (Time-Temperature-Transformation) and of crystallized fraction as a function of time or temperature.

To verify that the differences in conditions (size, surface effect, impurities) have little influence on the crystallization rates, the TTT curves obtained from inclusions in an industrial product were compared to ones from synthetic inclusions. In valve spring steel, spherical glassy inclusions, with diameters ranging from 2 to 35 μm, can be observed in an as-cast sample. Although all of them do not have exactly the same global composition, the dispersion is rather small. Isothermal heat treatments were done in reducing atmosphere (H_2+N_2). The inclusions were further observed with a SEM on a polished section: their crystallization rate depends on holding temperature and time. The phases were identified by their composition (EDS analysis): residual glassy phase, spinel (Al_2O_3-MgO) and anorthite (CaO-Al_2O_3-2SiO_2 or CAS_2) phases. The beginning of crystallization is noted if at least one of the inclusions observed (about 10 inclusions / cm^2) contains at least one crystal. The time at which the first crystals appear is drawn on figure 1. The curve is parabolic-shaped shape with τ_{nose} the minimal incubation time (5 minutes) at a temperature T_{nose} which is in the range 1150-1200°C on Figure 1.

A composition similar to the average composition of the inclusions was synthesized and similar heat treatments were performed. The crystallization curve is also reported on figure 1 for comparison with the results relative to endogenous inclusions. The crystallization temperature intervals are identical and the time for appearance of the first crystals has the same magnitude. The time difference may be due to slight composition differences and to the fact that the total observed oxide surface is lower in the product (a few μm^2).

It has thus been shown that the conditions undergone by the inclusions in the industrial product are similar to the conditions that prevail with synthetic oxide mixtures in a steel crucible. The experimental study with synthetic oxide mixtures is thus a good simulation of the transformations taking place in the steel samples and can be used to determine relevant tendencies as a function of heat treatment or inclusions compositions.

The small amounts of oxygen and water remaining in the crucible during TIG welding have probably reacted with the steel inner walls before crystallization, so that the oxygen and water activities are similar in synthetic inclusions and in the steel products. The FeO formed by the reaction of oxygen with the steel can dissolve in the liquid oxide at high temperature. However, the increase of the FeO contained in the glass is, as expected, negligible.

Other techniques can be used to study the crystallization of oxide melts: Differential Thermal Analysis (DTA), hot microscope, single and double hot thermocouple[4]. Particular attention should be taken about the conditions that prevailed around the sample. Indeed, a strong influence of the gas phase (Ar, air, O_2, wet atm.) has experimentally been shown in various oxide systems (aluminate spinel, lithium silicate, etc.) when studying the crystal growth rate or

nucleation rate[5,6]. The hot thermocouple method is a very elegant and efficient experimental technique which gave valuable results when studying the crystallization behavior of mold slags in air [7,8]. Its accuracy with respect to time scale of precipitation may be more questionable for simulating inclusions or trapped flux behavior during the thermal treatment of steel where the oxygen activity is low.

Criteria of the glass forming ability

Many compositions of the CaO-Al_2O_3-SiO_2-MgO system, as well as the effect of the addition of MnO, Na_2O and CaF_2, were studied. The experimental results, summarized in Table 1, were compared to the tendencies predicted by the theories of glasses[9]. The criteria of glassy phase stability are: low liquidus temperature of the mixture, high viscosity at the temperature of the nose of the TTT curve, large difference of composition between the liquid phase and the crystalline phases, high value of the melting entropy.

These criteria as well as approximations of the nose temperature or the glass transition temperature (T_{nose}= 0.77 $T_{liquidus}$, T_g= 2/3 $T_{liquidus}$) make a relative classification of the various compositions possible a priori. A more precise classification can be made thanks to the expression of the critical quenching rate [R_c= ($T_{liquidus}$ - T_{nose})/ τ_{nose})] established by Uhlmann[9] in the case where the composition of the liquid is identical to the composition of the crystal:

$$R_C = \frac{A.T_l^2}{h(0.77.T_l)} \exp(-0.212.B).[1-\exp(\frac{-0.3.\Delta H_m}{RT_l})]^{3/4} \qquad (1)$$

where A = 4.10^4 J m^{-3} K^{-1}, $\eta(0.77\ T_l)$ is the viscosity at the temperature of the nose taken as $0.77.T_{liquidus}$, B a kinetic parameter, and ΔH_m is the melting enthalpy of the oxide.

The tendencies that may be deduced from these approximations are globally respected: for instance, as shown in Figure 2, τ_{nose} increases as the viscosity increases, as expected from equation (1). In this figure, the viscosity is calculated according to the model proposed by Urbain[10].

In equation (1) the temperature of the nose is approximated as 0.77 $T_{liquidus}$ as suggested by Uhlmann[9]. However, as can be checked in Table 1, the calculated ratio of our experimental nose temperature versus liquidus temperature is larger: the average value is 0.86±0.06. These results show that these approximations are helpful to classify the relative ability of different compositions to form glassy phases, but they are not accurate enough to be quantitatively predictive. Indeed, the inclusions often have a complex composition and large deviations in the rate of crystallization may be noted for small composition variations. As an example, when the MgO content is increased from 0 to 7 weight % in a CaO-Al_2O_3-SiO_2 mixture[3], it has been observed that the rate of crystallization becomes high at 1100°C only for MgO contents larger than 6%, while the values of physical properties entering into equation (1) show no drastic variations in the whole domain.

Driving force for crystallization

Two types of TTT curves (Figures 3 and 5) were observed depending on whether the composition is close to an eutectic composition or not. Such shapes result from the competition between nucleation, favored by low temperatures, and growth favored by higher temperatures.

The simplest case is the appearance of a single phase over the whole time and holding temperature range: then a parabolic-shaped curve is obtained (Figure 3). The presented example corresponds to the composition located in the primary crystallization domain of anorthite. Indeed, the calculated driving force for the precipitation of this phase remains very much higher than the others at all temperatures (Figure 4).

Concerning compositions close to eutectic points or valleys, different crystalline phases may appear successively in time, and the nature of these assemblies may depend on holding temperature (Figure 5). The crystallization curve then presents several noses. An interpretation of this observation is proposed: the crystalline phases will appear in the order of decreasing volume free energy change (standardized at 1 atom g) for the crystallization of an infinitesimal amount of the phase at the expense of the liquid phase. On Figure 6, the variations of free energy are represented as a function of the temperature for the three phases susceptible of crystallizing. Note that the phases that are the most susceptible of crystallizing are anorthite just below the liquidus temperature, then anorthite ($CaO\text{-}Al_2O_3\text{-}2SiO_2$ or CAS_2) and pseudo-wollastonite ($CaO\text{-}SiO_2$ or CS), and finally pseudo-wollastonite and gehlenite ($2CaO\text{-}Al_2O_3\text{-}SiO_2$ or C_2AS) at low temperatures. The order observed experimentally is found.

Although it has the highest driving force, wollastonite is not observed below 1050°C; this is likely to be due to the fact that it does not contain any alumina and that at low temperature the diffusion coefficients are so low that alumina cannot diffuse out of a given volume. The crystalline phase which appears then (C_2AS) has a high driving force and a composition containing all the species of the initial supercooled liquid.

Effect of TiO_2 or ZrO_2 addition to crystallization kinetics

TiO_2 or ZrO_2 are often used as nucleating agents for alumino-silicate glass ceramics[11,12]. Glass ceramic manufacturing is a different problem than the inclusions behavior: the thermal treatment is adapted to control the crystallization. Nucleation is enhanced at low temperature and crystal growth is enhanced by increasing the temperature to an optimal value. In such materials the nucleating agent needs to have a low solubility and is used as heterogeneous sites for a secondary nucleation of the main crystalline phase. According to some recent results, the role of TiO_2 and ZrO_2 is controversial. If TiO_2 can be successfully used as nucleating agent in SiO_2 rich melts, it was found not to act as a direct nucleating agent in basic liquid compositions[13,14] in which it is more soluble. In order to check an effect on flux composition, small amounts of TiO_2 (3 and 5.5%) and ZrO_2 (3%) have been added to a composition simulating mold flux droplet trapped in Al-killed steel (Table 2). It appears on the TTT diagrams (Figure 7 to 10) that the time of appearance of first crystal is only slightly modified and is larger for some of the temperature ranges with TiO_2 or ZrO_2.

In this complex mixture, the primary phase crystallizing depends on temperature and composition:

- between 950°C and 1000°C soda melilite (solid solution between $2CaO\text{-}Al_2O_3\text{-}SiO_2$ and $2CaO\text{-}Na_2O\text{-}Al_2O_3\text{-}4SiO_2$) crystals are observed in all samples, but its crystal fraction remains low (5%),
- at 900°C and below, cuspidine ($CaF_2\text{-}3CaO\text{-}2SiO_2$) is the main crystalline phase in all compositions with about 50% of the volume for long thermal treatment. When ZrO_2 is initially present in the melt, it is found in the cuspidine phase in substitution with silica (10

ZrO_2 weight %). Concerning the samples that contain TiO_2, $CaTiO_3$ crystals are observed as primary or secondary phase in competition with cuspidine. At least, a solid solution of carnegieite (Na_2O-Al_2O_3-$2SiO_2$) and sodium aluminate (Na_2O-Al_2O_3) crystallizes in the remaining liquid.

Figure 11 shows the result of the percentage change of crystalline phases as a function of time at 900°C of the four compositions. On sample C, the first phase to crystallize is cuspidine which occupies a maximum of 45% of the total volume. A plateau of about 70 min is observed on the crystallization rate. This plateau corresponds to the incubation time for the second phase carnegieite. A final value of 95% crystallized (45% cuspidine +55% carnegeite+5% remaining glass) is then reached after holding the sample more than 120 minutes at 900°C. Addition of TiO_2 and ZrO_2 does not decrease the incubation time of the first phase but increases the overall growth rate. Optical and SEM observations on samples containing TiO_2 or ZrO_2, show that the second phase (carnegieite or $CaTiO_3$) precipitates without a secondary incubation time.

Thus, TiO_2 and ZrO_2 additions have a controversial effect in our experiments. In agreement with results obtained elsewhere[13,14], these species stabilize the liquid phase as the calculated critical cooling rate is lower: 2.1, 0.4, 0.75 and 0.6 K s^{-1} respectively for C, C+3%TiO_2, C+6%TiO_2 and C+3%ZrO_2. However, once the nucleation begins the overall crystallization rate is higher. Moreover, it is noteworthy to mention that for continuous cooled samples, cuspidine needles can be observed nucleating and growing on a ZrO_2 particle (Figure 12). The solubility of ZrO_2 in mold flux is rather low and decreases with temperature, so if the ability of ZrO_2 to nucleate is high thanks to a high driving force, it can precipitate and then form particles for heterogeneous nucleation of other phases.

Discussion on crystallization mechanisms

Nucleation in our samples was often observed to be heterogeneous on the wall of the crucible or on bubbles trapped in the viscous liquid. A change in the dominant nucleation mechanism from heterogeneous to homogeneous is observed when MgO or TiO_2 is present in the melt. As an example, in the sample C+6%TiO_2, $CaTiO_3$ crystals can be observed randomly dispersed in the bulk liquid.

Crystal growth can be controlled by diffusion or interfacial reaction. Figure 13 shows the concentration profile between two cuspidine disks of three species in the sample C. Na that is not soluble in the crystalline phase is rejected at the interface and its concentration is higher than in the volume; Ca diffuse towards cuspidine crystals which contains 47.3% of Ca; Si concentration is rather similar in both phases (15.3% in cuspidine, 19% in the remaining liquid) so that the gradient is small. According to this profile, and as diffusion coefficients are rather small in liquid oxides, for disks of about 10µm thick, the growth appears to be diffusion controlled.

In oxide melts large cations such as barium or rare earth have a low diffusion coefficient in the silicate network. Thus, as long as these species are soluble in the liquid phase, crystallization can be retarded[15]. Such behavior is indeed observed when 7% La_2O_3 is substituted to CaO in a 40.6% SiO_2, 27% CaO, 20.% Al_2O_3 and 5% MgO melt. Such an addition may change the phase equilibria ($T_{liquidus}$, primary field of crystallization), but as long as La_2O_3 is not a part of the primary crystals, it has to diffuse out of the growing crystals. In our experiments, the incubation time of silicate phases C_2AS or CAS_2 is double with La_2O_3: 15 to 30 minutes at the temperature

of the nose 1050°C. For the same thermal treatment, the crystal fraction is about half of the sample without La_2O_3.

Model of crystallization kinetics

The fractional change or the TTT diagrams allows the crystallization to be analyzed using the Johnson-Mehl-Avrami equations[16]

$$\ln[-\ln(1-X)] = n\ln k + n\ln(t-t) \qquad (2)$$

where X is the crystallized fraction, k the rate constant, τ the incubation time, t the time and n the Avrami parameter. To fit the parameter with the experimental values, the incubation time needs to be calculated. Indeed, it has been shown that the calculated n value is very sensitive to the chosen value for τ[17]. Supposing n does not change with crystallization at a fixed temperature, then τ is a function of n:

$$t = \frac{l(n)t_{0.5} - t_{0.005}}{l(n)-1} \text{ with } l(n) = \left[\frac{\ln(1-0.005)}{\ln(1-0.5)}\right]^{1/n} \qquad (3)$$

where $t_{0.005}$ and $t_{0.5}$ are the times to reach 0.05 and 50% of crystal.

In the present study, the kinetic parameters of the JMA equation have been calculated at different temperatures with an optimization software minimizing the χ^2 value

$$c^2(n,k,t) = \frac{1}{n^{eff} - p}\sum_i w_i\left(X_{\exp} - X(t_i,n,k,t)\right)^2 \qquad (4)$$

where n^{eff} is the number of experimental data and p the number of parameters that can be fitted, ω_i is a degree of confidence for the i experimental value. The results are shown in Table 3 for the composition of Figure 3 with an Avrami exponent n very close to 2. According to Christian[16], nucleation and growth mechanisms are associated with n values. n=2 corresponds to an homogeneous nucleation with a non constant nucleation rate and to a diffusion controlled growth of two dimensional crystals. This is in agreement with our microscopic observations for this sample: disks like crystals which appear as needles on a cross section, and observations of diffusion profile around the crystals.

Nucleation and growth mechanisms may change with temperature for more complex crystallization behavior. For instance for the crystallization behavior shown in figures 5 or 7 to 10, in which several crystalline phases or crystal morphologies are present, a purely mathematical deconvolution of the TTT diagram would be hazardous, and the values of n parameters thus determined might loose all physical meaning. It is doubtful that an JMA approach would have predictive virtues in this case. Moreover, the change of these coefficients (Avrami parameter n, activation energy) with composition has still to be found.

Conclusion

In order to obtain the desired inclusion rheology during hot rolling, a first selection of suitable compositions may be done using physico-chemical values (phase diagrams, viscosity) and the stability criteria of the glassy phases. However this theoretical approach is not sufficiently precise for complex oxide systems and experiments are necessary to determine the temperature range of crystallization and the crystallization kinetics. Our laboratory technique simulates the

conditions that prevail in the steel products and is thus well adapted to predict the crystallization behavior of inclusions for different heat treatments.

The addition of TiO_2 or ZrO_2 as nucleating agents has been tested in complex mold flux compositions containing less than 30% of SiO_2. It has been found that it does not decrease the time of appearance of first crystals, and the overall crystallization rate is only slightly increased. However, evidence of ZrO_2 crystals serving as heterogeneous sites for cuspidine nucleation has been observed.

Acknowledgments

The authors thank F. Bonnet, G. Lovato, J.P. Téres and F. Ruby for their contributions.

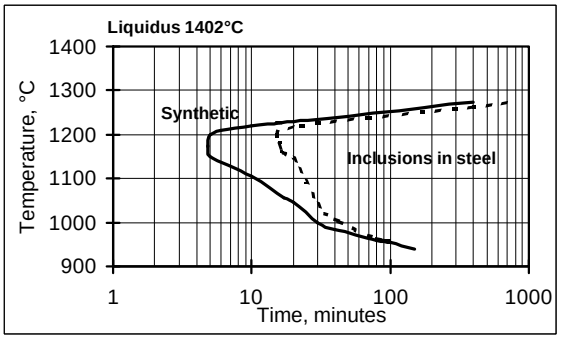

Figure 1: Appearance of the first crystals in the synthetic mixture (composition: 37.4 % SiO_2, 30.6 % CaO, 23.0 % Al_2O_3, 9.0 % MgO, solid line) and in endogenous inclusions of similar composition observed in industrial sample (dotted line).

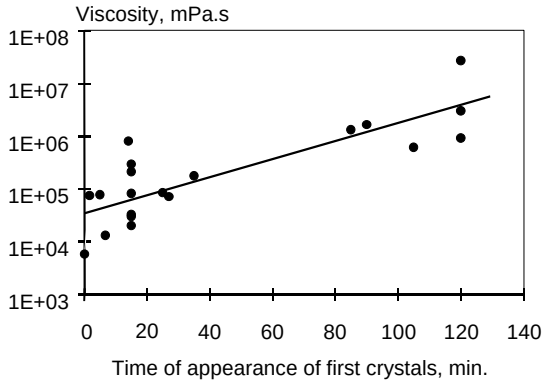

Figure 2: Relation between calculated viscosity at T_{nose} and time of appearance of first crystals. The points correspond to the compositions of Table I.

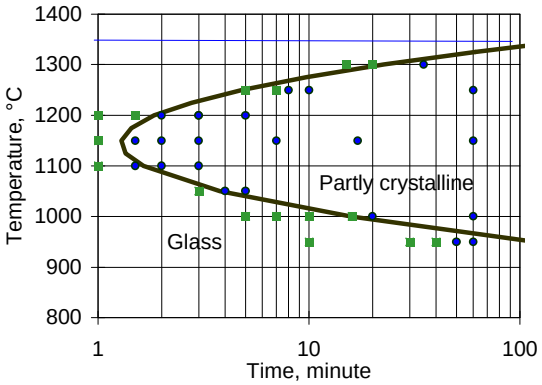

Figure 3: Crystallization behavior for the composition 41.3 % SiO_2, 33.7 % CaO, 24.5 % Al_2O_3 in anorthite field of crystallization.

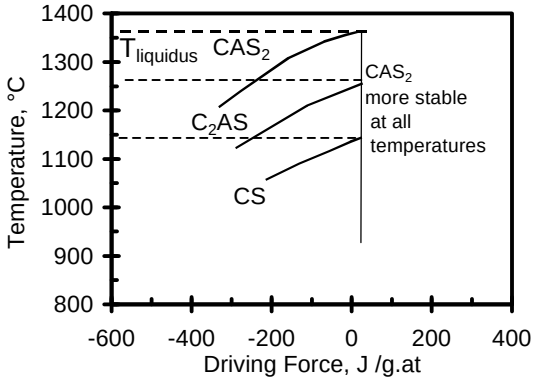

Figure 4: Evaluation of the volume free energy change for the formation of the various solids from the supersaturated liquid (composition of Figure 3).

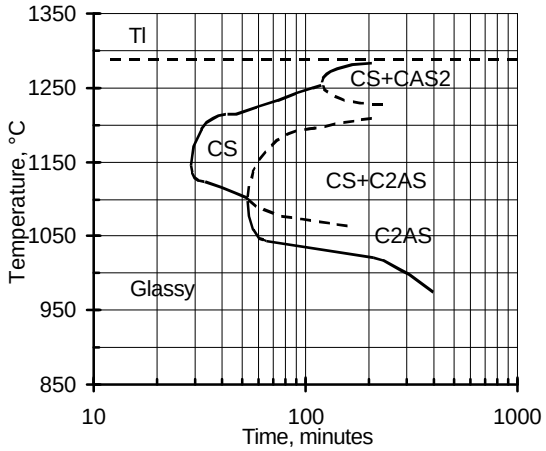

Figure 5: Crystallization behavior for the composition 41.3 % SiO_2, 38.2 % CaO, 20.0 % Al_2O_3 close to the ternary eutectic CS, C_2AS, CAS_2; TTT diagram.

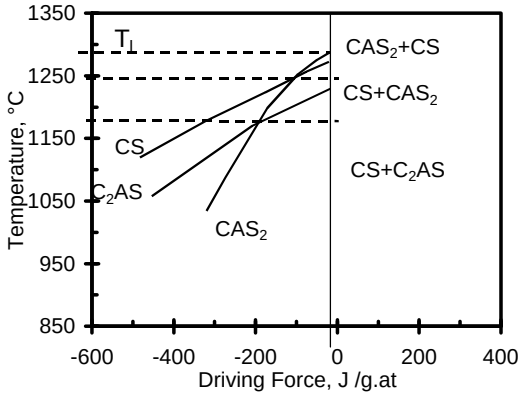

Figure 6: Evaluation of the volume free energy change for the formation of the various solids from the supersaturated liquid (composition of Figure 5).

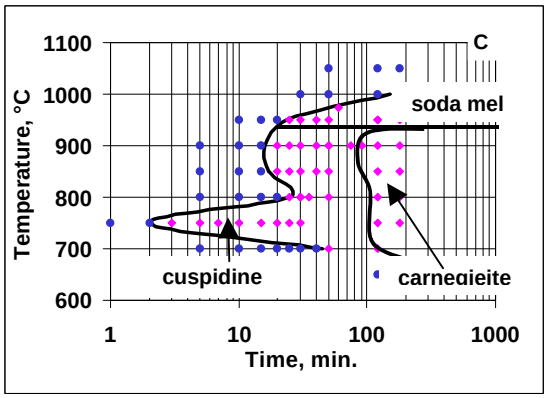

Figure 7 : TTT diagram for a slightly reduced mold flux (composition C in Table 2).

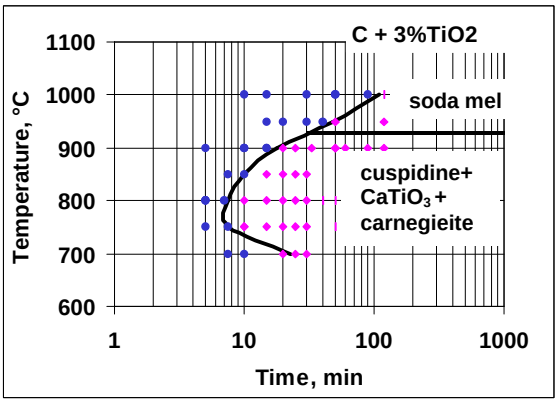

Figure 8 : TTT diagram for a slightly reduced mold flux (composition C+3%TiO_2 in Table 2).

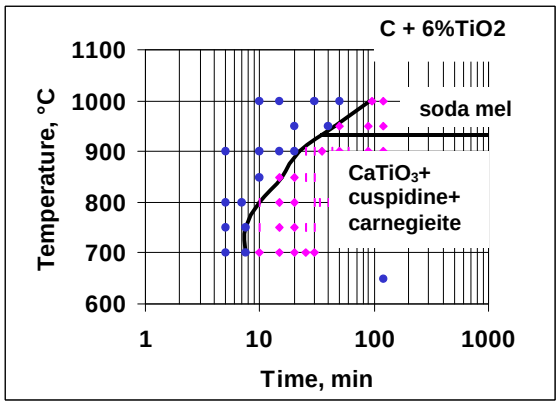

Figure 9: TTT diagram for a slightly reduced mold flux (composition C+6%TiO_2 in Table 2).

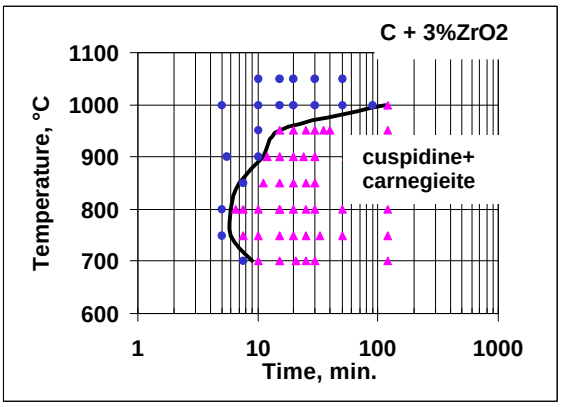

Figure 10: TTT diagram of a slightly reduced mold flux (composition C+3%ZrO_2 in Table 2).

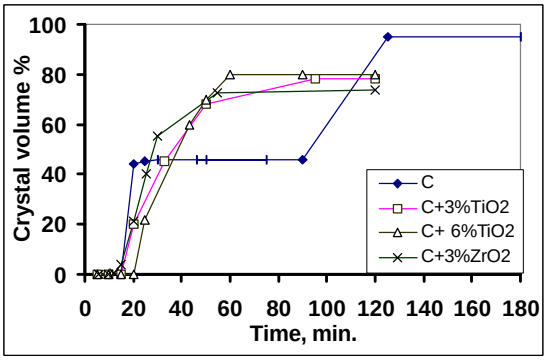

Figure 11: Crystal volume % versus time at 900°C. The plateau of sample C corresponds to the crystallization of cuspidine, the second crystal nucleation and growth is carnegieite. Composition in Table 2.

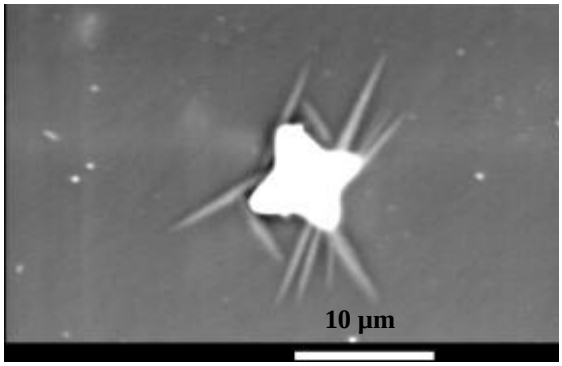

Figure 12: C + 3%ZrO_2 – cuspidine heterogeneous nucleation on ZrO_2 crystals containing 10 mass % CaO.

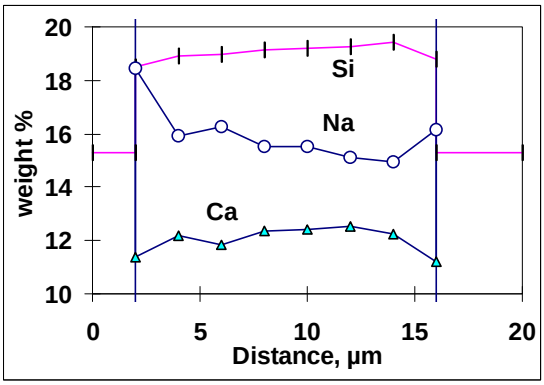

Figure 13 : Concentration profile between two cuspidine needles as measured by EDX. Composition C held 1h at 900°C

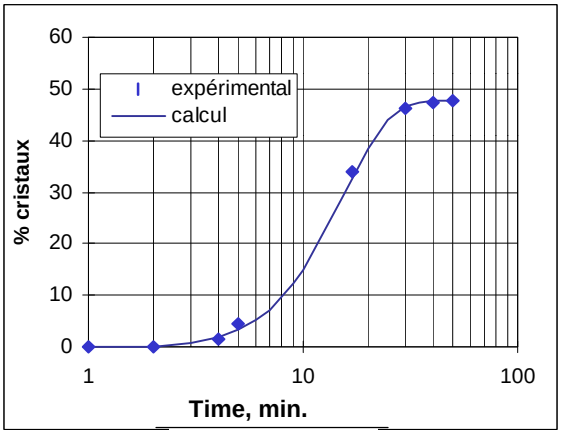

Figure 14 : Crystallization rate at T=1154°C for the composition A.

Table 1: Composition of synthetic slags (weight %), temperature of the measured nose(s), liquidus temperature and T_{nose}/T_l ratio for comparison with the expression $T_{nose} = 0.77\ T_l$.
The average of the values of $T_{nose}/T_l = 0.85 \pm 0.06$ is 10% higher than 0.77.
The first line corresponds to sample A, the second line to sample B.

SiO_2	CaO	Al_2O_3	MgO	T_{nose} , °C	$T_{liquidus}$, °C	T_{nose}/T_{liq}
41.3	33.7	24.5	0.25	1150	1360	0.871
41.3	38.2	20.0	0	1150	1347	0.913
42.5	35.7	21.2	0.4	1200	1305	0.934
				1025		0.823
40.6	34.0	20.3	5.1	1050	1387	0.797
39.9	33.5	20.0	6.1	1025	1396	0.763
				1000		0.778
39.5	33.4	19.5	7.3	1025	1408	0.772
42.2	34.4	20.6	2.8	1100	1343	0.910
60.9	21.7	17.0	0	1200	1219	0.931
				1000		0.804
39.0	31.9	24.2	4.95	1200	1380	0.891
				1000		0.770
56.7	21.1	17.2	5.1	1100	1196	0.935
				950		0.833
50.5	35.5	13.7	0	1300	1376	0.963
61.6	27.8	10.3	0	1100	1323	0.878
37.4	30.6	22.9	9.0	1175	1403	0.864
54.0	19.9	16.2	9.9	1050	1244	0.832

Table 2: Composition of slightly reduced mold flux and with addition of nucleating agents.

	C	C+3%TiO_2	C+6%TiO_2	C+3%ZrO_2
SiO_2	28.71	28.05	26.58	27.24
Al_2O_3	16.88	16.56	15.75	16.29
CaO	28.11	27.06	27.13	26.71
MgO	2.29	2.3	2.04	2.44
CaF_2	12.8	12.39	12.39	13.65
Na_2O	11.05	10.7	10.53	10.29
TiO_2	0.048	2.84	5.46	0.038
ZrO_2	0.004	0.004	0.004	3.24

Table 3: Kinetic parameters of equation (2) as determined for oxide mixture of composition A (T=1154°C).

Sample	k (min^{-1})	n	τ (min)	χ^2
A	0.071 ± 0.006	1.99 ± 0.31	1min42 ± 32s	10^{-4}

Table 4: Composition of the crystalline phases observed in the various samples analyzed. A= Al_2O3, N= Na_2O, C= CaO, S= SiO_2.

Crystalline phases	composition (weight %), for solids solutions limits of the compositions						
	SiO_2	Al_2O_3	CaF_2	CaO	MgO	Na_2O	TiO_2
anorthite	43.2	36.7		20.2			
wollastonite	51.7			48.3			
gehlenite C_2AS	21.9	37.2		40.9	0	0	
akermanite C_2MS_2	44.1	0		41.1	14.7	0	
soda-mélilite C_2NAS_4	46.6	19.8		21.7	0	11.8	
cuspidine C_3S_2F	32.8		21.3	45.9			
carnegieite NAS_2	42.2	35.9				21.8	
NA	32.2	45				25	
perovskite				41.2			58.8
spinel		71.8			28.2		

References

1) C. Gatellier, H. Gaye, J. Lehmann, Origine des inclusions dans les aciers peu alliés. Revue de Métallurgie, n°4 (1995), 541-553.

2) G. Bernard, P.V. Riboud, G. Urbain, Etude de la plasticité d'inclusions d'oxydes, La revue de Métallurgie 78 (5) (1981), 421-433.

3) P. Rocabois, J.N. Pontoire, H. Gaye, J. Lehmann, C. Gatellier, Crystallization of oxide inclusions and their rheology during hot rolling, Proc. of the 5th Clean Steel conf., 2-4 june 1997, Hungary, 120-129.

4) Y. Kashiwaya, C. E. Cicutti, A. W. Cramb, K.Ishii, Development of double and single hot thermocouple technique for in situ observation and measurements of mold slag crystallization, ISIJ Int. 38 (4), 348-356.

5) M. C. Weinberg ed., Nucleation and crystallization in liquids and glasses, Ceramic Transactions, vol. 30, The American Ceramic Society, 1993.

6) R. Chaim, A. H. Heuer, Crystallization in barium containing magnesium aluminosilicate glass-ceramic, J. Am. Ceram. Soc. 75 (6) (1992), 1512-21.

7) Y. Kashiwaya, C. E. Cicutti, A. W. Cramb, An investigation of the crystallization of a continuous casting mold slag using the single hot thermocouple technique, ISIJ Int. 38 (4), 357-365.

8) C. Orrling, A. Tilliander, Y. Kashiwaya, A. W. Cramb, Melting and solidification of mold slags, 82nd Steelmaking Conference proceedings (82), ISS, Chicago March 21-4, 1999, 417-424.

9) D. R. Uhlmann, N. J. Kreidl Eds, Glass: Science and Technology vol. 1, Academic Press, Inc., 1983.

10) G. Urbain, Viscosity estimation of slags, Steel Research 58 (3) (1987) 111-116.

11) J. Zarzycki, Les verres et l'état vitreux, Ed. Masson, 1982.

12) P.W. McMillan, Glass-Ceramics, Academic Press, 1964.

13) S. Jordery W. E. Lee, P. James, Crystallization hierarchy of CaO-P_2O_5-SiO_2-Al_2O_3-TiO_2 glass ceramics, J. Am. Ceram. Soc. 81 (9) (1998), 2237-44.

14) S. Morimoto, N. Kuriyama, Effect of TiO_2, ZrO_2 and P_2O_5 on the crystallisation of SiO_2-Al_2O_3-MgO-CaO-Na_2O glass system, Journal of the Ceramic Society of Japan, 104 [5] (1996) 466-468.

15) J-J. Shyu, C-H. Hwang, Effect of Y_2O_3 and La_2O_3 addition on the crystallization of $Li_2O.Al_2O_3.4SiO_2$ glass-ceramic, J. of Materials Science 31 (1996), 2631-39.

16) J.W. Christian, The theory of transformations in metals and alloys, Pergamon, New York, 1965.

17) M. Mao, Z. Altounian, Accurate determination of the Avrami exponent in phase transformation, Materials Science and Engineering, A149 (1991), L5-L8.